COMMUNICATION

Porous Nanoparticles

NANO · MICRO

small

www.small-journal.com

Check for updates

Mass Measurements Reveal Preferential Sorption of Mixed Solvent Components in Porous Nanoparticles

Mario M. Modena, Patrick Hirschle, Stefan Wuttke,* and Thomas P. Burg*

The interplay of physical and chemical properties at the nanometer scale provides porous nanoparticles with unique sorption and interaction capabilities. These properties have aroused great interest toward this class of materials for application ranging from chemical and biological sensing to separation and drug delivery. However, so far the preferential uptake of different components of mixed solvents by porous nanoparticles is not measured due to a lack of methods capable of detecting the resulting change in physical properties. Here, a new method, nanomechanical mass correlation spectroscopy, is used to reveal an unexpected dependence of the effective mass density of porous metal–organic framework (MOF) nanoparticles on the chemistry of the solvent system and on the chemical functionalization of the MOF's internal surface. Interestingly, the pore size of the nanoparticles is much too large for the exclusion of small solvent molecules by steric hindrance. The variation of effective density of the nanoparticles with the solvent composition indicates that a complex solvent environment can form within or around the nanoparticles, which may substantially differ from the solvent composition.

Porous nanoparticles are a unique class of materials that open many new opportunities in fields ranging from drug delivery and sensing to catalysis, green chemistry, and energy conversion.[1–8] Their physicochemical properties, in particular their morphology, surface charge, composition, porosity, and extremely high surface-to-volume ratio, are of paramount importance in defining their potential applications. Therefore, it is necessary to precisely

Dr. M. M. Modena, Dr. T. P. Burg
Max Planck Institute for Biophysical Chemistry
Am Faßberg 11, 37077 Göttingen, Germany
E-mail: tburg@mpibpc.mpg.de
P. Hirschle, Dr. S. Wuttke
Department of Chemistry and Center for NanoScience (CeNS)
University of Munich (LMU)
Butenandtstraße 11, 81377 Munich, Germany
E-mail: stefan.wuttke@cup.uni-muenchen.de
Dr. S. Wuttke
School of Chemistry
University of Lincoln
Joseph Banks Laboratories
Brayford Pool, Lincoln LN6 7DL, UK

The ORCID identification number(s) for the author(s) of this article can be found under https://doi.org/10.1002/smll.201800826.

control and measure these parameters.[4,9–17] Several characterization methods can be used to probe nanoparticles:[18,19] Nanometer-scale resolution on particle morphology and crystallinity can be obtained using solid-state approaches (e.g., electron microscopy and X-ray diffraction).[20] However, these methods can only be used on dry samples, and thus they cannot account for interactions between the nanoparticles and the suspending solution. Mobility-based methods (e.g., dynamic light scattering) are commonly used to measure the hydrodynamic radius and zeta-potential of nanoparticles in liquids.[19] Mobility, however, does not vary significantly with the internal state of nanoparticles, such as the filling of the pores. Therefore, pore volume, pore accessibility, and the internal affinity to specific gases are currently only probed in the dry state (e.g., nitrogen adsorption and helium pycnometry), or by the indirect measurement of the adsorption of probe molecules dissolved in solvents of different polarity.[21]

To circumvent this limitation, we used nanomechanical mass correlation spectroscopy (MCS)[22] to measure the effective mass density of metal–organic framework (MOF) nanoparticles in different solvent systems. In this approach, the MOF nanoparticles are dispersed in a range of binary solvent systems and the mass fluctuations resulting from the flow of this suspension through a suspended microchannel resonator (SMR) mass sensor of 10 pL volume are measured (1 pL = 10^{-12} L; **Figure 1**). We used materials institute lavoisier (MIL)-101(Cr) MOF nanoparticles[23] with different inner pore functionalizations and suspended them in binary mixtures of ethanol and water, and methoxyperfluorobutane (HFE-7100) and ethanol (EtOH). Based on geometry alone, these modifications of the solvent systems and of the functionalization of the pores are not expected to change the mass of the nanoparticles. The observed differences therefore provide new information about the specific interaction between the different solvent components and the internal surface.

MIL-101(Cr) nanoparticles are mesoporous MOF nanoparticles featuring two types of cages with respective diameters of 2.9 and 3.4 nm, and an accessible window of 1.2 and 1.4 nm.[23] Here, we have examined the effective density of three different MIL-101(Cr) species: MIL-101(Cr) nanoparticles and MIL-101(Cr) derivatives functionalized at the coordinatively unsaturated metal sites with pyridine or pyrazine using postsynthetic modification.[24] The crystallinity, porosity, and morphology of the MIL-101(Cr) nanoparticle species were investigated with powder X-ray diffraction (PXRD) (Figure S3,
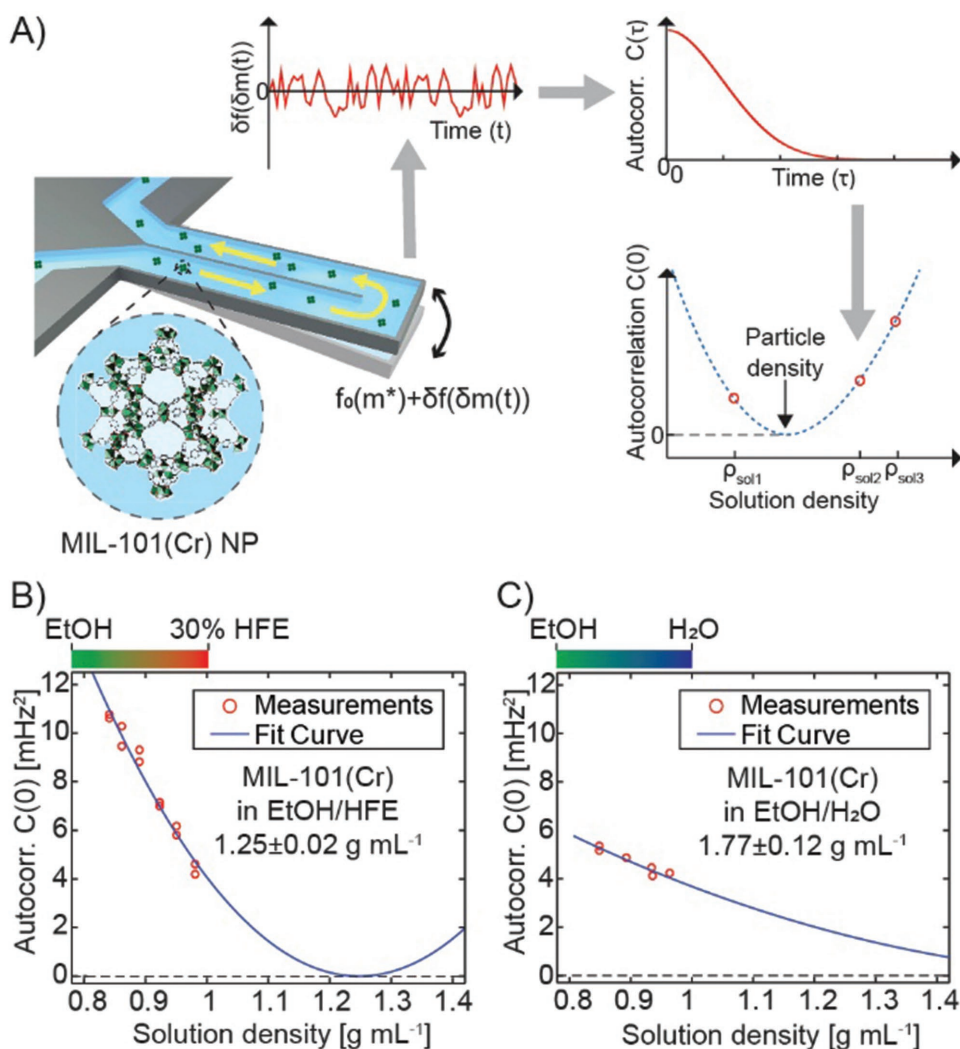
Figure 1. Density characterization of MIL-101(Cr) nanoparticles. A) Direct mass measurements with suspended microchannel resonators reveal the mass density of porous nanoparticles in different mixed solvents. Particles flowing through a microfluidic channel embedded into a nanomechanical resonator cause resonance-frequency variations proportional to the induced mass fluctuations. These mass fluctuations are measured with high precision by correlation analysis. B) Variation of the magnitude $C(0)$ of the autocorrelation for the MIL-101(Cr) nanoparticle signal in mixtures of HFE-7100/EtOH with a solution density ranging from 0.84 g mL^{-1} ($\approx$8% HFE-7100) to 0.98 g mL^{-1} ($\approx$30% HFE-7100). The measured density of the particles is 1.25 ± 0.02 g mL^{-1}; C) The density of MIL-101(Cr) nanoparticles in polar solvents was measured by using a mixture of 50×10^{-3} M Glycine-HCl (pH 2.5)/EtOH, with density ranging from 0.85 g mL^{-1} ($\approx$76% EtOH) to 0.96 g mL^{-1} ($\approx$2% EtOH). A buffer solution with low pH was selected as the MIL-101(Cr) nanoparticles present higher stability and low aggregation when suspended in acid conditions (Figure S17, Supporting Information).

Supporting Information), nitrogen adsorption/desorption isotherms (Table S6, Supporting Information), (trasmission and scanning electron microscopy, TEM, Figures S4–S7, Supporting Information; SEM, Figures S8–S13, Supporting Information), respectively. We characterized the nanoparticles using both SEM of dried ethanolic suspensions, resulting in a size distribution of $d^{SEM} = (41 \pm 10)$ nm (Figures S14–S16, Supporting Information), and dynamic light scattering (DLS) in ethanol yielding in a hydrodynamic diameter of $d^{DLS} = (105 \pm 31)$ nm (Figure S18, Supporting Information).

The density of MIL-101(Cr) nanoparticles was measured using both apolar and polar solvents to probe the behavior of particles when exposed to different solvent mixtures (Figure 1). Surprisingly, the effective mass density of the particles depends significantly on the solvent

system. In the relatively apolar mixture of HFE-7100 with EtOH, MIL-101(Cr) nanoparticles present a density $\rho_{eff}^{HFE/EtOH} = 1.25 \pm 0.02$ g cm^{-3} (Figure 1b), while their density increases to $\rho_{eff}^{EtOH/Water} = 1.77 \pm 0.12$ g cm^{-3} (Figure 1c) in the more polar mixture of ethanol with an aqueous buffer (50×10^{-3} M Glycine-HCl, pH 2.5). Both values are much larger than the mass density of the empty framework, which can be calculated from the crystal structure as $\rho^{empty} = 0.66$ g cm^{-3} (Figure S21, Supporting Information).

Next, we modified MIL-101(Cr) nanoparticles using a post-synthetic grafting approach. The coordinatively unsaturated chromium sites (Lewis acid sites) are used to coordinate Lewis bases,[24] pyrazine or pyridine, to render the particles more hydrophilic or hydrophobic, respectively (**Figure 2**). As for the unfunctionalized MIL-101(Cr) nanoparticles,

ADVANCED
SCIENCE NEWS
www.advancedsciencenews.com

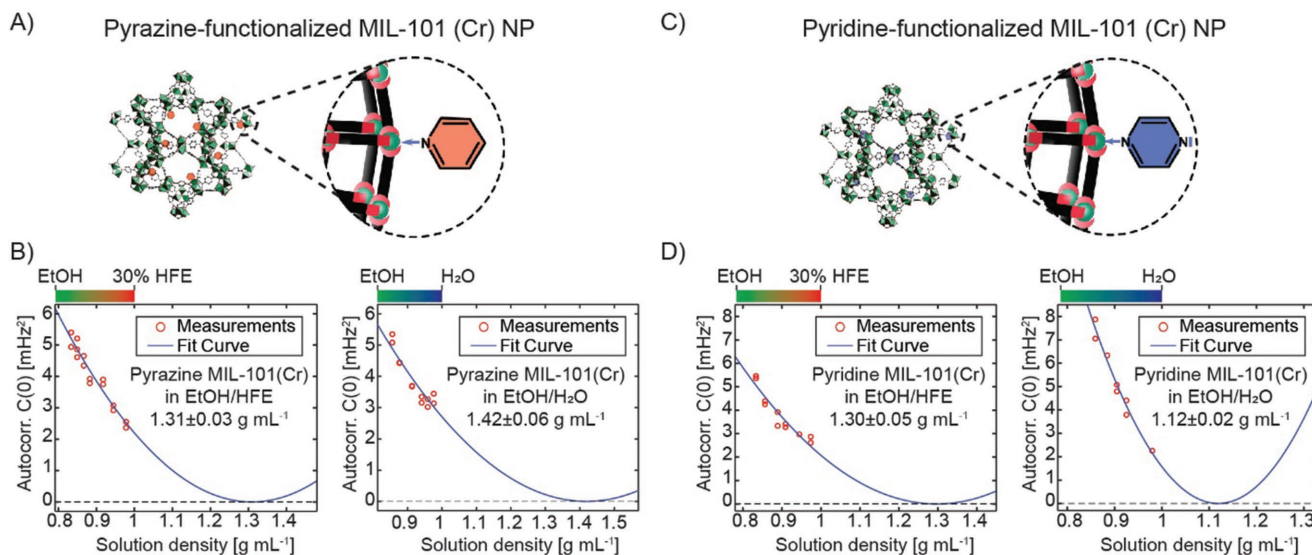NANO · MICRO
small
www.small-journal.com

Figure 2. Density measurements of functionalized MIL-101(Cr) nanoparticles. A) MIL-101(Cr) nanoparticles were functionalized with pyrazine at the coordinatively unsaturated metal sites. B) Density measurements of pyrazine-functionalized MIL-101(Cr) particles suspended in mixtures of HFE-7100/EtOH (left) and 50×10^{-3} M Glycine-HCl/EtOH (right). The particles present an unexpected higher effective density in the polar mixture; C) The hydrophobicity of MIL-101(Cr) nanoparticles was increased by functionalization of the inner and outer-surface area with pyridine. D) Density characterization of the pyridine-functionalized MIL-101(Cr) particles in mixtures of HFE-7100/EtOH (left) and 50×10^{-3} M Glycine-HCl/EtOH (right).

the measurements were carried out in mixtures of HFE-7100/EtOH and of 50×10^{-3} M Glycine–HCl (pH 2.5)/EtOH to detect both the particle densities and their permeability to the solvents in solution. Measurements in the HFE-7100/EthOH mixtures return an effective density of $\rho_{eff}^{HFE/EtOH} = 1.31 \pm 0.03$ g cm^{-3} for the pyrazine-functionalized particles and $\rho_{eff}^{HFE/EtOH} = 1.30 \pm 0.05$ g cm^{-3} for the pyridine-functionalized particles.

These results are in line with the values found for the unfunctionalized MOF nanoparticles. More pronounced differences are detected when measuring the density of the functionalized nanoparticles in the polar mixture. For the pyrazine-functionalized nanoparticles, we find a surprisingly high effective density of $\rho_{eff}^{EtOH/Water} = 1.42 \pm 0.06$ g cm^{-3} in the mixture of ethanol and water (Figure 2b). As for the measurements of the unfunctionalized MIL-101(Cr) nanoparticles, the uncertainty on the effective density increases with the value of the estimated density. In contrast, the pyridine-functionalized nanoparticles show a drastic decrease in effective density to $\rho_{eff}^{EtOH/Water} = 1.12 \pm 0.02$ g cm^{-3} when suspended in the same mixture (Figure 2d). The lower effective density may be due to an increased ethanol content within the particles. This could occur due to particle aggregation with concomitant inclusion of ethanol in the interstitial volume and/or due to the formation of an ethanol solvation layer surrounding the nanoparticles. In both cases, the ethanol fraction may be locally increased in the aqueous mixture because of the hydrophobic functional groups presented both on the inner and outer surface of the nanoparticles. This hypothesis is supported by DLS measurements of the nanoparticles suspended in the two mixtures: the nanoparticles in ethanol have a hydrodynamic diameter of 96 nm (polydispersivity 18%), while their size increases to 149 nm (polydispersivity 40%) in a 95% 50×10^{-3} M Glycine-HCl/5% ethanol mixture.

The density estimations obtained for the different cases of MIL-101(Cr) nanoparticles when suspended in the different solvent mixtures are summarized in **Table 1**. The observed dependence of mass density on the chemical identity of the solvent in MOF nanoparticles can be understood by considering the possible interactions of the solvent components with the pore volume. Our measured correlation signal $C(0)$ represents the variance of the resonance frequency fluctuations of the SMR. This is directly proportional to the variance of mass fluctuations arising from Poisson statistics, i.e., $C(0) \sim c_0 V \cdot \left. \frac{\partial \rho}{\partial c} \right|_{\mu}^{2}$, where c_0 denotes the solid concentration, $V = 10$ pL is the volume, and $\left. \frac{\partial \rho}{\partial c} \right|_{\mu}$ is the density increment of the solution at constant chemical potential. In the simplest case, when particles are described as hard spheres, the density increment follows Archimedes' law

$$\left. \frac{\partial \rho}{\partial c} \right|_{\mu} = 1 - \frac{\rho_s}{\rho_{eff}} \tag{1}$$

Table 1. Summary of density estimations for the functionalized and unfunctionalized MIL-101(Cr) MOF nanoparticles in the different solvent mixtures.

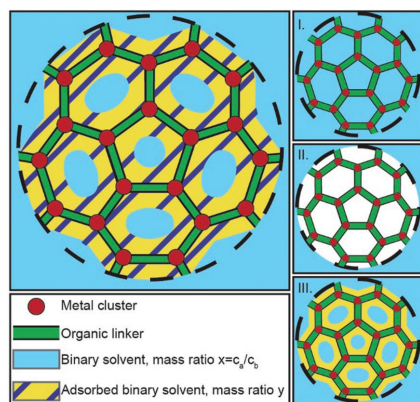| MIL-101(Cr) functionalization	Solvent mixture	
	EtOH/HFE [g cm^{-3}]	EtOH/50×10^{-3} M Glycine-HCl [g cm^{-3}]
Unfunctionalized	1.25 ± 0.02	1.77 ± 0.12
Pyrazine-functionalized	1.31 ± 0.03	1.42 ± 0.06
Pyridine-functionalized	1.30 ± 0.05	1.12 ± 0.02

Figure 3. Schematic representation of the selective sorption of mixed solvents into porous MOF nanoparticles. The dashed line symbolizes the outer perimeter of the nanoparticle with dry mass M_f and total volume V_p. In the most general case, different solvent components can freely access only a fraction of the pore volume (shown in light blue). Here the mass ratio x of solvent components matches that of the surrounding fluid. In another part of the internal volume, the composition is altered by specific interactions between the different solvent components and the solid framework (yellow/blue hatched region). The mass ratio y of solvent components in this region can differ significantly from the surrounding fluid. Three special cases of this model are of particular interest: I) All solvent components can freely access the entire pore volume. II) Nonsolvent molecules can access the internal volume. III) One of the solvent components (light yellow) can access a larger portion of the internal volume than the other.

where ρ_s is the mass density of the solvent and ρ_{eff} denotes the mass density of the solid, which is equal to the inverse partial specific volume of the particles. In this case, the autocorrelation curve presents zero amplitude when the density of the suspending solution matches the density of the particles.

Porous nanoparticles present a fundamentally different behavior. In solution, their effective density depends not only on their dry mass and volume but also on the ability of the solvent to access the pore volume. There can be significant differences in pore accessibility for different solvent components due to size exclusion and more complex interactions, such as solvation effects and gating. All of these phenomena may alter the effective mass density of the particles and necessitate an extension of the pure physical/geometric description, which is inherent to Archimedes' principle.

To explain the range of the observed differences, we represent the pore volume by two compartments, as shown in **Figure 3**. Note that this is done only for modeling purposes; in reality, there need not be a defined physical boundary. In the first compartment (light blue) the solvent composition tracks the composition outside the pore exactly. In contrast, the composition in the second compartment (blue/yellow in Figure 3) is fixed and given by specific adsorption or exclusion of individual solvent components. The dry mass of the particle is increased by the fixed mass of adsorbed solvent molecules. This leads to the following expression for the density increment

$$\left.\frac{\partial \rho}{\partial c}\right|_{\mu} = (1 + B_A + B_B)\left(1 - \frac{\rho_s}{\rho'_{eff}}\right) \qquad (2)$$

where the adsorption coefficients B_A and B_B denote the mass fractions of the solvent components A and B, respectively, that are bound to the particles.[25,26] The total adsorbed mass fraction is $(B_A + B_B)$ and the effective mass density of the particles is given by

$$\rho'_{eff} = \frac{1 + B_A + B_B}{\rho_f^{-1} + B_A \rho_A^{-1} + B_B \rho_B^{-1}} \qquad (3)$$

Note that ρ_f represents the density of the nanoparticle framework and depends on the accessibility of the pores to the solvent. To illustrate different scenarios, we consider three special cases. First, if the particles are fully permeable (case I), $B_{A,B} = 0$ and ρ'_{eff} is given by Equation (3) and $\rho_f = \frac{M_f}{V_f}$ (Figure 3,I), where M_f is the dry mass of one particle and V_f is the volume occupied by the framework. In our experiments with MIL-101(Cr) nanoparticles, this yields a value of $\rho'_{eff} = 3.1$ g cm^{-3} based on a pore volume fraction of 79% calculated from the crystal structure (Figure S21, Supporting Information). Second, if the particles are impermeable (case II), the solid particle model applies with $\rho_{eff} = \frac{M_f}{V_p}$ (Figure 3,II), where V_p is the hard-sphere volume of one particle. In this case, the crystal structure reveals a value $\rho_{eff} = 0.66$ g cm^{-3}. Finally, if one solvent component, e.g., component A, permeates selectively (case III), then $B_B = 0$ and $B_A > 0$ (Figure 3,III).

The wide range of effective density values corresponding to these cases explains the differences we observe in the different experiments. Although the measurements do not provide sufficient information to extract each of the parameters (ρ_f, B_A, and B_B) individually for the different solvent systems and particle functionalizations, the observed variation in density establishes that their combination differs significantly in each of the measured cases, with case I and II not being supported by our experimental findings.

Our results show that tuning the inner functionalization of porous MOF nanoparticles can produce considerably different local compositions of the solvent mixtures within and/or around the nanoparticles. This capability opens interesting new opportunities for the use of MOF nanoparticles, such as separation of solvent mixture based on selective enhancement of a solvent component in the pores.

Finally, the novel density method presented here can be applied to any other porous nanoparticle system, which will greatly advance our understanding of one key physicochemical parameter of porous nanoparticles and open up a broad spectrum of applications of this class of materials, from separation to biomedical science.

Experimental Section

Density Measurements: Density of particles in solution is measured by detecting the variation of buoyant mass when the particles are suspended in mixtures of different concentrations of ethanol and 50×10^{-3} M Glycine-HCl (pH = 2.5) or ethanol and HFE-7100. The test solutions are injected into a suspended microchannel resonator featuring an embedded channel with a cross-section of 3×8 μm^2. The resonance frequency of the resonator is measured by using

an optical-lever detection scheme (see Figure S1, Supporting Information, for more information on the experimental setup). During the measurement, particle concentration is kept constant to simplify the subsequent data analysis process. As the buoyant mass of the particles is proportional to the induced frequency fluctuations, the time-domain mass signal is first high-pass filtered (cutoff frequency = 1 Hz) to remove slow-term-noise fluctuations, caused by temperature and/or mechanical variations. Frequency fluctuations are then analyzed by use of an autocorrelation analysis of the high frequency domain to minimize the effect of the uncorrelated readout noise background. The effective density of the particles is calculated after fitting the autocorrelation amplitude as a function of solution density, with the estimated particle density corresponding to the minimum of the fitting parabola. Therefore, the uncertainty on density estimation depends on the range of solution densities accessed during the measurement. More information on and validation measurements of the density characterization method are reported in the Supporting Information.

Synthesis of MIL-101(Cr) Nanoparticles: The synthesis of MIL-101(Cr) was conducted using microwave (MW) assisted synthesis.[27] A mixture of $Cr(NO_3)_3 \cdot 9H_2O$ (1.48 g, 3.70 mmol) and terephthalic acid (0.615 g, 3.70 mmol) was added to water (20 mL, Milli-Q) and stirred until all $Cu(NO_3)_3 \cdot 9H_2O$ was dissolved. Subsequently, the reaction mixture was placed in a Teflon tube (80 mL) and sealed. The tube was placed in a microwave oven (*Synthos 3000, Anton-Paar*) along with 3 other vessels, two of them filled with water (20 mL) and one acting as control vessel and filled with an aqueous $Cu(NO_3)_3 \cdot 9H_2O$ (1.48 g, 3.70 mmol) solution. The solutions were first heated for 4 min to reach 210 °C and then were kept for 2 min at this temperature. A cooling phase of 1.5 h was then performed to allow the solutions to reach room temperature. The resulting nanoparticles were washed via centrifuging (20 500 rpm, 45 min), removal of supernatant, and then redispersing them in ethanol (30 mL) under sonication. Subsequently the MOF nanoparticle dispersion was filtered to remove the excess terephthalic acid. This washing procedure was performed, in total, four times for ensuring complete wash of the produced particles.

Postsynthetic Functionalization with Pyridine and Pyrazine: MIL-101(Cr) nanoparticles were functionalized by linking of pyrazine or pyradine functional groups to the coordinatively unsaturated metal sites using a postsyntethic functionalization strategy. For the pyrazine functionalization, an ethanolic MIL-101(Cr) nanoparticle dispersion (7.2 mL, c = 12.4 mg mL^{-1}) was added to an ethanolic pyrazine solution (7.2 mL, c = 320 mg mL^{-1}, 4×10^{-3} M). The reaction mixture was kept stirring for 24 h. The resulting modified nanoparticles were washed in four cycles consisting of centrifuging (14 000 rpm, 30 min), removal of supernatant and redispersing in ethanol under sonication.

Similarly for the pyridine functionalization, pyridine (12.2 mL, 154 mmol) was added to an ethanolic MIL-101(Cr) nanoparticle dispersion (7.2 mL, *c* = 12.4 mg mL^{-1}) in addition to ethanol (2.2 mL). The reaction mixture was kept stirring for 24 h. The resulting modified nanoparticles were washed in four cycles consisting of centrifuging (14 000 rpm, 30 min), removal of supernatant and redispersing in ethanol under sonication.

Characterization of MIL-101(Cr) Nanoparticles: The synthetized functionalized and unfunctionalized MIL-101(Cr) nanoparticles were characterized using dynamic light scattering, zeta-potential measurements, scanning electron microscopy, transmission electron microscopy, thermogravimetry, powder X-ray diffraction, and nitrogen sorption. Detail description of the characterization methods and results are reported in the Supporting Information.

Supporting Information

Supporting Information is available from the Wiley Online Library or from the author.

Conflict of Interest

The authors declare no conflict of interest.

[1] X. Meng, B. Gui, D. Yuan, M. Zeller, C. Wang, *Sci. Adv.* **2016**, *2*, e1600480.

[2] M. Zhao, K. Deng, L. He, Y. Liu, G. Li, H. Zhao, Z. Tang, *J. Am. Chem. Soc.* **2014**, *136*, 1738.

[3] B. Ghalei, K. Sakurai, Y. Kinoshita, K. Wakimoto, A. P. Isfahani, Q. Song, K. Doitomi, S. Furukawa, H. Hirao, H. Kusuda, S. Kitagawa, E. Sivaniah, *Nat. Energy* **2017**, *2*, 17086.

[4] G. Lu, S. Li, Z. Guo, O. K. Farha, B. G. Hauser, X. Qi, Y. Wang, X. Wang, S. Han, X. Liu, J. S. DuChene, H. Zhang, Q. Zhang, X. Chen, J. Ma, S. C. J. Loo, W. D. Wei, Y. Yang, J. T. Hupp, F. Huo, *Nat. Chem.* **2012**, *4*, 310.

[5] S. Wuttke, M. Lismont, A. Escudero, B. Rungtaweevoranit, W. J. Parak, *Biomaterials* **2017**, *123*, 172.

[6] H. Furukawa, U. Müller, O. M. Yaghi, *Angew. Chem., Int. Ed.* **2015**, *54*, 3417.

[7] Z. Li, J. C. Barnes, A. Bosoy, J. F. Stoddart, J. I. Zink, *Chem. Soc. Rev.* **2012**, *41*, 2590.

[8] M. W. Tibbitt, J. E. Dahlman, R. Langer, *J. Am. Chem. Soc.* **2016**, *138*, 704.

[9] C. Walkey, J. Olsen, H. Guo, A. Emili, W. Chan, *J. Am. Chem. Soc.* **2012**, *134*, 2139.

[10] H. Furukawa, N. Ko, Y. B. Go, N. Aratani, S. B. Choi, J. Kim, O. M. Yaghi, *Science* **2010**, *329*, 424.

[11] S. Wuttke, A. Zimpel, T. Bein, S. Braig, K. Stoiber, A. Vollmar, D. Müller, K. Haastert-Talini, J. Schaeske, M. Stiesch, G. Zahn, A. Mohmeyer, P. Behrens, O. Eickelberg, D. A. Bölükbas, S. Meiners, *Adv. Healthcare Mater.* **2017**, *6*, 1.

[12] S. A. MacParland, K. M. Tsoi, B. Ouyang, X. Z. Ma, J. Manuel, A. Fawaz, M. A. Ostrowski, B. A. Alman, A. Zilman, W. C. W. Chan, I. D. McGilvray, *ACS Nano* **2017**, *11*, 2428.

[13] Y. Sakata, S. Furukawa, M. Kondo, K. Hirai, N. Horike, Y. Takashima, H. Uehara, N. Louvain, M. Meilikhov, T. Tsuruoka, S. Isoda, W. Kosaka, O. Sakata, S. Kitagawa, *Science* **2013**, *339*, 193.

[14] H. Goesmann, C. Feldmann, *Angew. Chem., Int. Ed.* **2010**, *49*, 1362.

[15] B. Rungtaweevoranit, Y. Zhao, K. M. Choi, O. M. Yaghi, *Nano Res.* **2016**, *9*, 47.

[16] S. Xu, Z. Nie, M. Seo, P. Lewis, E. Kumacheva, H. A. Stone, P. Garstecki, D. B. Weibel, I. Gitlin, G. M. Whitesides, *Angew. Chem., Int. Ed.* **2005**, *44*, 724.

[17] J. Ma, A. P. Kalenak, A. G. Wong-Foy, A. J. Matzger, *Angew. Chem., Int. Ed.* **2017**, *56*, 14618.

[18] P. Hirschle, T. Preiß, F. Auras, A. Pick, J. Völkner, D. Valdepérez, G. Witte, W. J. Parak, J. O. Rädler, S. Wuttke, *CrystEngComm* **2016**, *18*, 4359.

[19] C. Y. Tay, M. I. Setyawati, J. Xie, W. J. Parak, D. T. Leong, *Adv. Funct. Mater.* **2014**, *24*, 5936.

[20] J. Park, H. Elmlund, P. Ercius, J. M. Yuk, D. T. Limmer, Q. Chen, K. Kim, S. H. Han, D. A. Weitz, A. Zettl, A. P. Alivisatos, *Science* **2015**, *349*, 290.

[21] M. Sin, C. Kutzscher, I. Senkovska, T. Ben, S. Qiu, S. Kaskel, E. Brunner, *Microporous Mesoporous Mater.* **2017**, *251*, 129.

[22] M. M. Modena, Y. Wang, D. Riedel, T. P. Burg, *Lab Chip* **2014**, *14*, 342.

[23] G. Férey, C. Mellot-Draznieks, C. Serre, F. Millange, J. Dutour, S. Surblé, I. Margiolaki, *Science* **2005**, *309*, 2040.

[24] S. Wuttke, C. Dietl, F. M. Hinterholzinger, H. Hintz, H. Langhals, T. Bein, *Chem. Commun.* **2014**, *50*, 3599.

[25] P. H. Brown, A. Balbo, H. Zhao, C. Ebel, P. Schuck, *PLoS One* **2011**, *6*, e26221.

[26] H. Eisenberg, *Biophys. Chem.* **2000**, *88*, 1.

[27] S. Wuttke, S. Braig, T. Preiß, A. Zimpel, J. Sicklinger, C. Bellomo, J. O. Rädler, A. M. Vollmar, T. Bein, *Chem. Commun.* **2015**, *51*, 15752.

1800826 (6 of 6)